RSC Advances

PAPER

View Article Online
View Journal | View Issue

Cite this: *RSC Adv.*, 2021, **11**, 28863

Ultrathin porous amine-based solid adsorbent incorporated zeolitic imidazolate framework-8 membrane for gas separation

Yu Qin, Li Xu, Liying Liu, Xiaoyu Deng, Yucheng Gao and Zhongwei Ding *

A novel gas separation approach is proposed in this work by combining an amine-based solid adsorbent with a zeolitic imidazolate framework-8 (ZIF-8) membrane. This was achieved by incorporating the amine-based solid adsorbent during the fabrication of the ZIF-8 membrane on a macroporous substrate. An amine-based solid adsorbent was prepared using porous ZIF-8-3-isocyanatopropyltrimethoxysilane (IPTMS) and *N*-[(3-trimethoxysilyl)propyl]diethylenetriamine (3N-APS) amine compounds. The as-prepared porous amine-based solid adsorbent (denoted as ZIF-8-IPTMS-3N-APS) possessed excellent adsorptive CO_2/N_2 and CO_2/CH_4 separation performances. As the adsorbent needs to be regenerated, this could indicate that the CO_2 adsorption separation process cannot be continuously operated. In this work, an amine-based solid adsorbent was applied during the preparation of the ZIF-8 membranes owing to the following reasons: (i) gas separation by the membrane can be operated continuously; (ii) the amino group provides a heterogeneous nucleation site for ZIF-8 to grow; and (iii) the reparation of surface defects on the macroporous substrate can be performed prior to the growth of the ZIF-8 membrane. Herein, the ZIF-8 membrane was successfully fabricated, and it possessed excellent CO_2/CH_4, CO_2/N_2, and H_2/CH_4 separation performances. The 0.6 μm ultrathin ZIF-8 membrane demonstrated a high CO_2 permeance of 4.75×10^{-6} mol m^{-2} s^{-1} Pa^{-1} at 35 °C and 0.1 MPa, and ideal CO_2/N_2 and CO_2/CH_4 selectivities of 4.67 and 6.02, respectively. Furthermore, at 35 °C and 0.1 MPa, the ideal H_2/CH_4 selectivity of the ZIF-8 membrane reached 31.2, and a significantly high H_2 permeance of 2.45×10^{-5} mol m^{-2} s^{-1} Pa^{-1}.

Received 21st June 2021
Accepted 15th August 2021

DOI: 10.1039/d1ra04801e

rsc.li/rsc-advances

1. Introduction

The carbon capture and storage (CCS) process has recently emerged as an increasingly important topic owing to the worsening issue of global warming.[1,2] This process requires efficient separation of CO_2, one of the main greenhouse gases, from exhaust gas streams. During the CCS process, CO_2/CH_4 and CO_2/N_2 separation in post-combustion and pre-combustion CO_2 capturing are usually involved.[3] To achieve the separation of CO_2 in exhaust gas streams, membrane technologies have been employed, and these technologies have been able to demonstrate continuous operational durability.[4] Currently, various membranes, such as polymers,[5] mixed matrices,[6] facilitated transport,[7] zeolites,[8] and carbon molecular sieve membranes,[9] have been applied in the separation of CO_2. Despite their generally motivating performances, these membranes exhibit certain inherent disadvantages that significantly hinder their mass adoption in industrial-level production. For instance, polymeric membranes present a dilemma between the selectivity and permeability, mixed matrix membranes suffer from poor compatibility between the polymer matrix and the selective molecular sieve particles, and facilitated transport membranes can be easily poisoned by impurities.[10–12] Thus, owing to these limitations, there remains a strong need to explore alternative membranes that can be used effectively in CCS.

As a subclass of metal–organic frameworks (MOFs), zeolitic imidazolate frameworks (ZIFs) are extensively used as molecular sieving membranes owing to their tunable pore sizes, excellent porosity, and thermal/chemical stability.[13] Among the various ZIFs, zeolitic imidazolate framework-8 (ZIF-8) possesses sodalite (SOD) topology, with a pore size of *ca.* 0.34 nm.[14,15] It should be noted that the pore size of ZIF-8 is slightly larger compared to the kinetic diameter of CO_2 (0.33 nm), while it is smaller as compared to those of CH_4 (0.38 nm) and N_2 (0.364 nm). Consequently, owing to this suitable pore size, ZIF-8 is theoretically beneficial in the separation of CO_2/N_2 and CO_2/CH_4 pairs. Even though ZIF-8 may present an excellent opportunity in CCS owing to its pore size, the lattice flexibility of the ZIF-8 membranes typically leads to a poor separation performance, as indicated by the selectivity (ratio of the permeability of gas i and gas j).[4] To enhance the selectivity of i and j, it is

Beijing Key Laboratory of Membrane Science and Technology, College of Chemical Engineering, Beijing University of Chemical Technology, Beijing 100029, China. E-mail: dingzw@mail.buct.edu.cn; Tel: +86-10-64436781

essential to increase the difference in the gas permeability. Additionally, it is noted that gas permeability can be affected by the gas adsorption capacity, whereby a higher adsorption capacity generally results in a higher permeability in the membrane separation system. Thus, increasing the CO_2 adsorption capacity can enhance the CO_2 permeability, which in turn benefits the separation performances of CO_2/CH_4 and CO_2/N_2. This strategy has been demonstrated in numerous previously reported gas separation studies on the membrane technique.[14,16–18] Recently, Sasikumar *et al.* reported polysulfone membranes that encompass amine-modified SiO_2/ZIF-8 nanofillers for CO_2/CH_4 and CO_2/N_2 separation and they found that the high CO_2 affinity of the amine group allowed the selective transport of CO_2 rather than CH_4 and N_2.[19] Consequently, it is crucial to select a specific amine-modified porous material that possesses an excellent CO_2 adsorption capacity and can also be applied in the preparation of the ZIF-8 membrane.

An amine-based solid adsorbent is often employed in the adsorption and separation of CO_2 owing to its desirable CO_2 adsorption capacity.[20,21] Generally, amine-based solid adsorbents are divided into three categories; amine compounds of class 1 adsorbents involve physical adhesion onto the surface of the porous support, while amine compounds of the class 2 and class 3 adsorbents are chemically attached to the pore walls.[22] When compared to class 2 and 3, the class 1 adsorbent is theoretically easier to prepare. However, owing to the weak physical interaction between the amine compound and the porous support, this can easily lead to amine leaching, which ultimately limits the stability of the class 1 adsorbent.[23] The leaching of the amine in class 1 adsorbents for CO_2 capturing applications was initially reported by Jones *et al.*[24] According to their report, clogging of the adsorption column with leaching species was observed, and this led to a sharp reduction in the CO_2 adsorption capacity of tetraethylenepentamine (TEPA)-impregnated mesoporous silica (SBA-15) after the first cycle, and this decreased continuously in the following cycles. In contrast, class 2 and class 3 adsorbents are able to achieve a better stability and higher CO_2 adsorption capacities as the amine molecules are chemically bonded to the raw porous support. For instance, Chang and co-workers synthesized aminosilane-modified mesoporous silica for the adsorption of CO_2.[25] According to their work, the aminosilane-modified mesoporous silica was able to achieve a high CO_2 adsorption capacity of 2.41 mmol g^{-1} at 333 K. Huang *et al.* also prepared a CO_2 adsorbent by modifying mesoporous silica MCM-48 with 3-aminopropyltriethoxy-silane.[26] Their reported material was able to demonstrate the highest reported CO_2 adsorption capacity of 2.05 mmol g^{-1} at 298.15 K and 100 kPa. Although these reports have generally revealed the possibility of using amine-based solid adsorbents for the separation of CO_2, the regeneration process for the adsorbent typically requires the consumption of energy. As such, even though the energy needed for the regeneration process has been reduced with recent advances, this limitation can still severely hinder the continuous operation of the adsorbents in industrial applications.[27–30] Thus, a novel strategy is proposed in this work by incorporating an amine-based adsorbent into the preparation process of the ZIF-8 membrane for CO_2 separation. This proposed CO_2 separation strategy can be operated continuously without the need for regeneration owing to the inherent advantages of the membrane separation process. Furthermore, the amine-based adsorbent should provide an excellent CO_2 adsorption capacity that can help to enhance the inherently poor CO_2/N_2 and CO_2/CH_4 separation performances exhibited by the pristine ZIF-8 membrane.

As for the preparation of the ZIF-8 membranes, various methods have been used, which are conventionally divided into two categories: *in situ* growth and secondary growth.[31] For these two methods, the formation of ultrathin ZIF-8 membranes and the strong adhesion between the ZIF-8 membrane and the substrate are challenging. Several studies have been reported in which the ZIF-8 membrane was synthesized and overcome these challenges through innovative techniques. Zhao *et al.* successfully controlled the thickness of the ZIF-8 membrane layer within 1 μm through the current-driven synthesis method.[32] Meanwhile, the strong adhesion between the ZIF-8 membrane and the substrate was also achieved owing to the formation of the ZIF-8 layer in the porous channels of the substrate. Yue and co-workers prepared ZIF-8 thin membranes through transformation of the ZnO nanoscopic precursors and the connection strength between the ZIF-8 membrane and the substrate was improved.[33] However, it is essential to develop a more energy-efficient and versatile synthesis method for ZIF-8 membranes. It is worth mentioning that ZIF-8-3-isocyanatopropyltrimethoxysilane (IPTMS) hybrid materials have recently been demonstrated for the fabrication of an ultrathin ZIF-8 membrane and the adhesion between the ZIF-8 membrane and the substrate was strengthened.[34] In addition, the porous ZIF-8-IPTMS is highly suitable for use as a raw porous support for the preparation of class 2 solid adsorbents owing to the high hydroxyl group content on the surface, which act as reaction sites for the grafting of amines. As such, the as-prepared class 2 solid adsorbent is expected to serve as a multifunctional deposition layer during the fabrication of ZIF-8 membranes.

Herein, the amine-based solid adsorbent was fabricated from ZIF-8-IPTMS hybrid materials and 3N-APS amine compounds. Based on these results, the as-prepared adsorbent, denoted as ZIF-8-IPTMS-3N-APS, when applied in the fabrication of ZIF-8 membranes, offers numerous advantages over the pristine ZIF-8-IPTMS. Firstly, the loading of the amine compounds provided more heterogeneous nucleation sites for the ZIF-8 membranes to grow. Secondly, the weakly alkaline amine compounds can enhance the adsorption capacities of the material towards acidic CO_2, without significantly affecting its adsorption capacities towards both the nonacidic N_2 and CH_4. Such a distinction in the adsorption capacities is conducive to achieving a more efficient separation performance for the ZIF-8 membranes. Lastly, the incorporation of the amine-based adsorbent into the fabrication process of the ZIF-8 membranes for CO_2 separation can facilitate the enhancement of the CO_2/CH_4 and CO_2/N_2 separation performances. Furthermore, this incorporation could also ensure the ability of the membrane to operate continuously, which is an important

requirement in industrial applications. Thus, based on these findings, the strategy proposed in this work could have a promising future in CCS applications.

2. Experimental

2.1. Materials

A ceramic α-Al_2O_3 tube, with a length, inner diameter, and outer diameter of 100, 9, and 13 mm, respectively, was supplied by Foshan Ceramics Research Institute of China. Toluene ($\geq$99.5%) and anhydrous methanol ($\geq$99.5%) were purchased from Tianjin Damao Chemicals. IPTMS ($\geq$97%), zinc nitrate hexahydrate ($Zn(NO_3)_2 \cdot 6H_2O$, $\geq$99%), and 2-methyl imidazole (HmIM, 99%) were procured from Aladdin. *N*-[(3-Trimethoxysilyl)propyl]diethylenetriamine (3N-APS, 97%) agent was obtained from Thermo Fisher Scientific. The chemicals were used in the experiment as received, and the deionized water (DI water) used in this experiment was made in the lab.

2.2. Preparation of ZIF-8-IPTMS

ZIF-8-IPTMS was synthesized using ZIF-8 crystals and IPTMS silane coupling agents based on the procedures reported in our previous work.[34] In a typical preparation process, ZIF-8 (0.1 g), IPTMS (1 g), and DI water (100 g) were first incorporated into a round-bottom flask. After which, the mixture was heated at 110 °C for 1 h in an oil bath with a reflux condenser. Subsequently, the reaction system was subjected to centrifugation to collect the white product. Then, DI water was used to repeatedly wash the product. Lastly, the washed product was dried at 100 °C under vacuum conditions for 5 h, and it was later ground into a powder, which was denoted as ZIF-8-IPTMS.

2.3. Fabrication of ZIF-8-IPTMS-3N-APS

The as-prepared ZIF-8-IPTMS was later modified with 3N-APS amine compounds with various volume concentrations. Inspired by a previous report, the volume concentrations of the 3N-APS amine compounds were fixed as 10 vol%, 15 vol%, and 20 vol%.[35] In a typical preparation process, ZIF-8-IPTMS (2.0 g) was added into toluene that contained varying amounts of 3N-APS. Then, the mixture was refluxed at 110 °C for 24 h. After which, the reaction system was subjected to centrifugation to retrieve the product. Subsequently, the product was washed with toluene repeatedly. Lastly, the washed product was dried at 80 °C in vacuum conditions overnight, and then it was ground to a powder for subsequent use. Hereafter, the products were denoted as ZIF-8-IPTMS-3N-APS-*X* (in which *X* represents the volume concentration of the 3N-APS used). For instance, ZIF-8-IPTMS-3N-APS-15 indicates the sample prepared with 15 vol% 3N-APS.

2.4. Depositing ZIF-8-IPTMS-3N-APS-15 on a macroporous α-Al_2O_3 tube

To ensure the smoothness of the surface, the exterior of the macroporous α-Al_2O_3 tube was polished with three grades of sandpaper successively, for example, #500, #800, and #1200. After which, anhydrous methanol was used to eliminate the impurities from the surface of the tube. Subsequently, a facile slip-coating method was performed to deposit ZIF-8-IPTMS-3N-APS-15 onto the surface of the tubular substrate. Simply, the substrate was activated at 150 °C for 3 h and then the activated substrate was later immersed in 1 wt% ZIF-8-IPTMS-3N-APS-15 suspension for 20 s with magnetic stirring. Lastly, the substrate was dried at 60 °C for 12 h.

2.5. Preparation of the ZIF-8 membrane

ZIF-8 membrane was fabricated based on a previously published process.[36] In a typical preparation process, Zn $(NO_3)_2 \cdot 6H_2O$ (0.44 g) and HmIM (9.08 g) were respectively added into deionized water (80 ml), and it was continuously stirred until a homogenous solution was obtained. Then, the ZIF-8-IPTMS-3N-APS-15 coated substrate was introduced into a Teflon-lined hydrothermal reaction vessel vertically, together with all the above-prepared solutions. After which, the hydrothermal process was conducted at 120 °C for 7 h. After which, the hydrothermal product was washed with anhydrous methanol thoroughly. Finally, the washed product was soaked in anhydrous methanol solution overnight. This membrane preparation process was repeated to mend the defects on the product.

2.6. Characterizations

The morphologies of ZIF-8-IPTMS and ZIF-8-IPTMS-3N-APS and the thickness of the as-fabricated ZIF-8 membrane were investigated using scanning electron microscopy (SEM, Hitachi, S4800). The crystal structure of the sample was determined using X-ray diffractometry (XRD, Ultima IV, Rigaku). Fourier transform infrared spectroscopy (FTIR, Nicolet 8700) was performed to analyze the chemical functional groups in the samples. Thermogravimetric analysis (TG, TGA/DSC3+) was conducted to evaluate their thermal stabilities. The specific surface area and BJH (Barrett, Joyner, and Halenda) pore size of the materials were determined by recording their N_2 adsorption–desorption isotherms with a volumetric adsorption analyzer (ASAP 2460). The CO_2, N_2, and CH_4 adsorption performances of these hybrid materials were recorded at 308 K. The CO_2 adsorption separation performance of ZIF-8-IPTMS-3N-APS was obtained by conducting breakthrough experiments at 308 K and 0.1 MPa for the CO_2/CH_4 (85/15 v/v) and CO_2/N_2 (85/15 v/v) gas mixtures.

2.7. Gas permeation

Fig. 1a shows the schematic illustration of a single gas permeation experiment. Before the gas permeation experiment, the sample was first rinsed with anhydrous methanol and then desiccated in a vacuum oven at 50 °C for 6 h. Subsequently, it was activated under a continuous flow of inert gas. Various gases, for example, CH_4 (0.38 nm), N_2 (0.364 nm), CO_2 (0.33 nm), and H_2 (0.289 nm), were used to investigate the gas separation performance of the membrane. During the experiment, 0.1, 0.2, 0.3, and 0.4 MPa were successively set as the transmembrane pressure, and 35 °C was set as the experiment

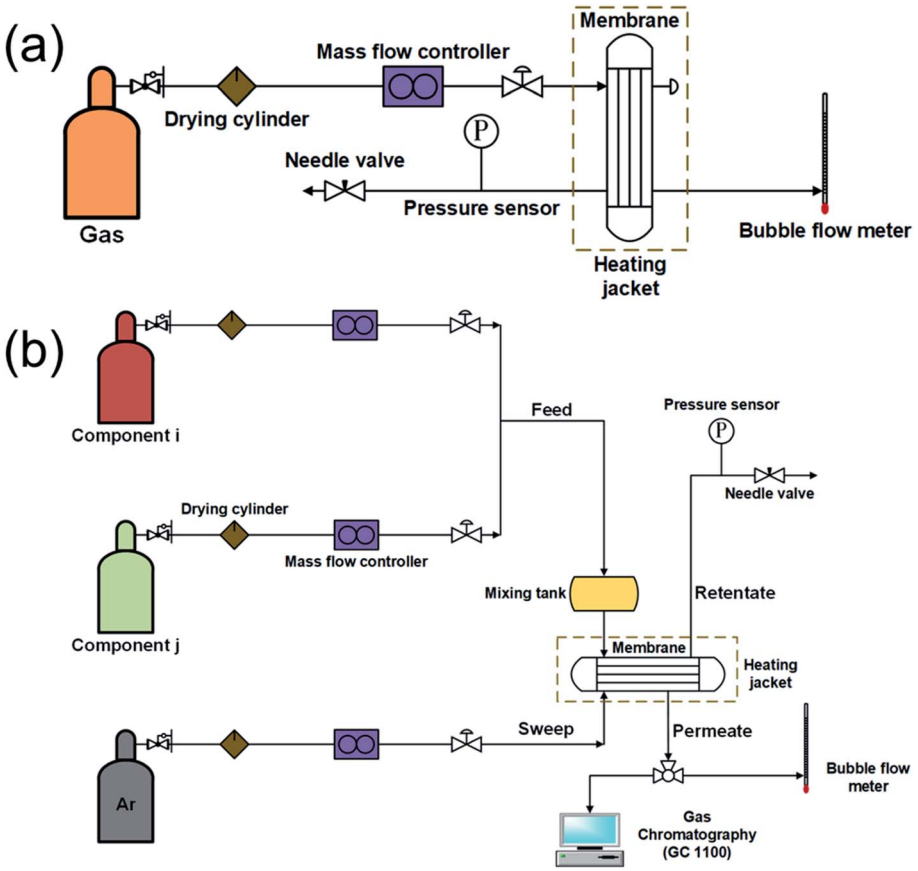

Fig. 1 Schematic illustration of (a) the single and (b) the binary gas permeation experiment set up based on the Wicke–Kallenbach technique.

temperature. The permeance P_i of the permeant gas i can be described using the following equation:

$$P_i = \frac{N_i}{\Delta P_i \cdot A} \quad (1)$$

In which ΔP_i represents the pressure difference across the membrane of component i (Pa), N_i represents the permeating flux of component i (mol s^{-1}), and A represents the area of the membrane (m^2). The ideal selectivity $\alpha_{i,j}$ can be determined according to the following equation:

$$\alpha_{i,j} = \frac{P_i}{P_j} \quad (2)$$

As shown in Fig. 1b, the binary gas permeation test was performed for the sample *via* the Wicke–Kallenbach method. During this test, the temperature and the transmembrane pressure were maintained at 35 °C and 0.1 MPa, respectively. CO_2/CH_4 (85/15 v/v), CO_2/N_2 (85/15 v/v), and H_2/CH_4 (50/50 v/v) gas mixtures were applied to the feed side. Gas chromatography (GC1100) was then employed to determine the compositions of the feed streams and the permeate, with argon gas serving as the sweep gas. The separation factor $\alpha_{i/j}$ of gas i and gas j can be determined using the following equation:

$$\alpha_{i/j} = \left(\frac{y_{i,perm}/y_{j,perm}}{x_{i,feed}/x_{j,feed}}\right) \quad (3)$$

In which x indicates the molar fraction of the component in the feed, and y indicates the molar fraction of the component in the permeate.

3. Results and discussion

3.1. Comparing ZIF-8-IPTMS and ZIF-8-IPTMS-3N-APS

According to the SEM results shown in Fig. 2a, ZIF-8-IPTMS possessed a spherical morphology, which is consistent with our previous research.[34] SEM analysis was also conducted for ZIF-8-IPTMS-3N-APS prepared by modifying ZIF-8-IPTMS with various volume concentrations of 3N-APS amine compounds, and the images are shown in Fig. 2b–d. As shown in the results, the as-prepared ZIF-8-IPTMS-3N-APS retained the spherical morphology and appropriate size, which are advantageous to the reparation of surface defects on the macroporous substrate. More importantly, it could be observed that ZIF-8-IPTMS-3N-APS-15 was comprised of more particles, which results from the attachment of numerous 3N-APS amine compounds on the surface of ZIF-8-IPTMS.[37]

Fig. 3a presents the FTIR spectra of the ZIF-8-IPTMS and ZIF-8-IPTMS-3N-APS. The peak located at *ca.* 1640 cm^{-1} is

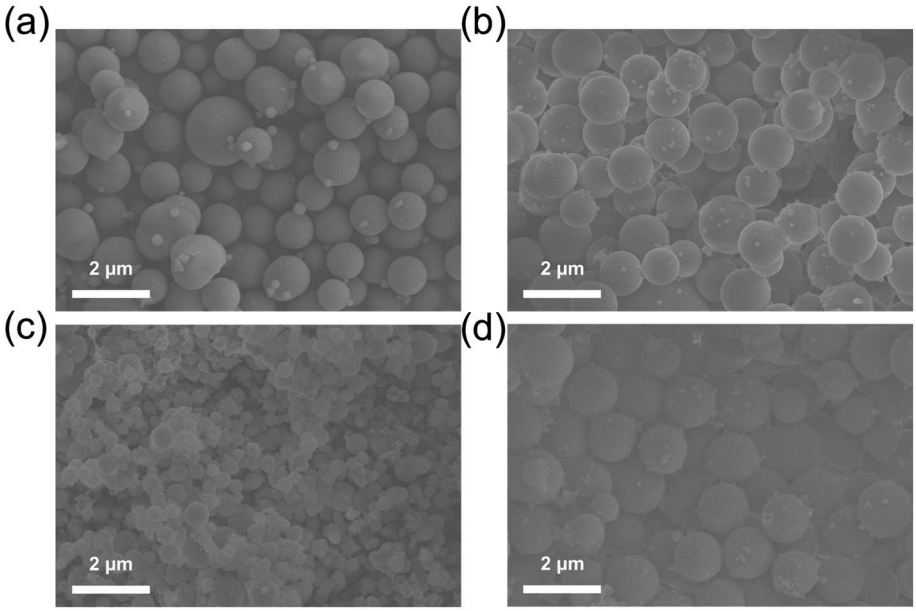

Fig. 2 SEM results of (a) ZIF-8-IPTMS, (b) ZIF-8-IPTMS-3N-APS-10, (c) ZIF-8-IPTMS-3N-APS-15, and (d) ZIF-8-IPTMS-3N-APS-20.

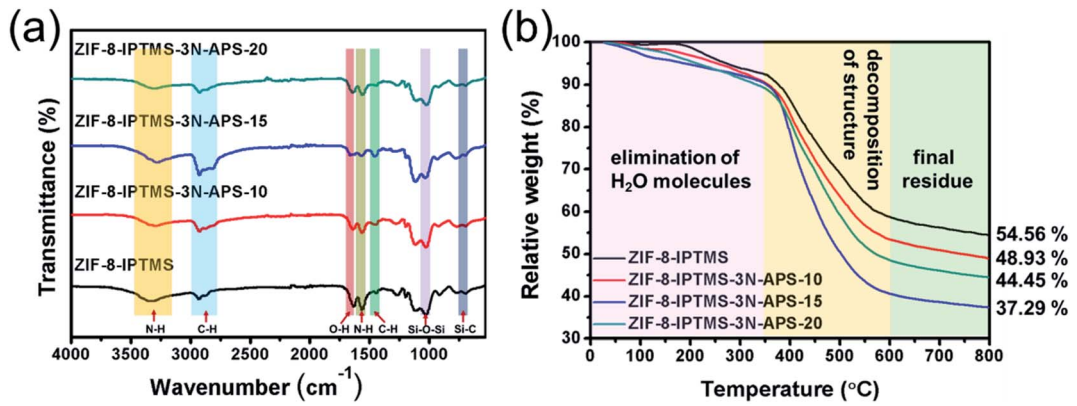

Fig. 3 (a) FTIR spectra, and (b) TG profiles of ZIF-8-IPTMS, ZIF-8-IPTMS-3N-APS-10, ZIF-8-IPTMS-3N-APS-15, and ZIF-8-IPTMS-3N-APS-20.

associated with the surface hydroxyl group (–OH) stretching vibration in pristine ZIF-8-IPTMS.[38] After subjecting ZIF-8-IPTMS to refluxing treatment for 24 h, the intensity of this peak was weakened, this is mainly attributed to the reaction between the surface hydroxyl group in ZIF-8-IPTMS with the alkoxy ligand in the 3N-APS amine compounds.[39] Meanwhile, the intensities of the bands located at 2880–2970 cm^{-1} (C–H stretching in $CH_2CH_2CH_2$–NH_2 group) and around 1450 cm^{-1} (alkane C–H deformation vibrations) were strengthened.[40,41] An infrared (IR) peak with a reduced intensity located at 1569 cm^{-1} (N–H scissoring vibration in secondary amines) and enhanced peaks located at 3300–3370 cm^{-1} (symmetric/asymmetric N–H stretching vibrations of hydrogen-bonded amino groups) could also be observed.[40–43] Based on the changes in these peak intensities, it can be concluded that 3N-APS was successfully decorated on the surface of ZIF-8-IPTMS. To determine the temperature at which ZIF-8-IPTMS and ZIF-8-IPTMS-3N-APS decomposed, TGA was performed, and the results are shown in Fig. 3b. A minor weight loss below 350 °C could be observed for these hybrid materials owing to the elimination of the surface-adsorbed water.[44] According to previous research, the initial decomposition point of the grafted amine bearing chain is at 300 °C, and it is stable below this temperature.[39] Thus, it is clear that the significant difference in the weight loss for these hybrid materials in the temperature range of 350 to 600 °C could be ascribed to the elimination of their structural and surface functional groups.[40] Hence, the amine loading content could be confirmed by the weight loss recorded within the temperature range of 350 to 600 °C. In general, a higher weight loss would indicate a higher amine loading content. Based on the above-mentioned characterization analyses, the largest amount of 3N-APS was bound onto the surface of ZIF-8-IPTMS when the volume concentration of the 3N-APS amine compound used was 15 vol%. This conclusion may be owed to

the inability of a lower volume concentration of 10 vol% to achieve a sufficient grafting effect, while a higher volume concentration of 20 vol% may lead to an excessive occurrence of self-consumable condensation reactions among the 3N-APS amine compounds.

Fig. 4a–d shows the N_2 adsorption–desorption isotherms of ZIF-8-IPTMS and ZIF-8-IPTMS-3N-APS. The initial steep slope at $P/P_0 < 0.08$ can be ascribed to the type I isotherm, which indicates that ZIF-8-IPTMS and ZIF-8-IPTMS-3N-APS are both microporous materials.[45] Based on the BJH pore size distribution profiles shown in Fig. 4e, ZIF-8-IPTMS and ZIF-8-IPTMS-3N-APS both possess a pore size of *ca.* 1.8 nm. As such, according to these results, the grafting of amine compounds onto the ZIF-8-IPTMS does not exert a significant impact on its pore structure. Retention of the pore with a large diameter can facilitate the subsequent operation, whereby it involves the reparation of the surface defects on the macroporous support during the ZIF-8 membrane preparation process, and at the same time achieving a high gas permeation. Interestingly, the surface areas of the ZIF-8-IPTMS-3N-APS hybrid materials were reduced to *ca.* 30 $m^2\ g^{-1}$ after being modified with amine compounds, which were significantly lower than those of the pristine ZIF-8-IPTMS hybrid materials (171 $m^2\ g^{-1}$). This significantly reduced surface area can be mainly ascribed to the fact that the pore walls of pristine ZIF-8-IPTMS were partly clogged by the grafted 3N-APS amine compounds. This result dramatically decreases the adsorption capacities of nonacidic gases other than acidic CO_2, and therefore could provide a better CO_2 separation performance.

Fig. 5a–d shows the single-component gas sorption isotherms, for example, CO_2, N_2, and CH_4, of ZIF-8-IPTMS and ZIF-8-IPTMS-3N-APS at 308 K. The CO_2 adsorption capacities of

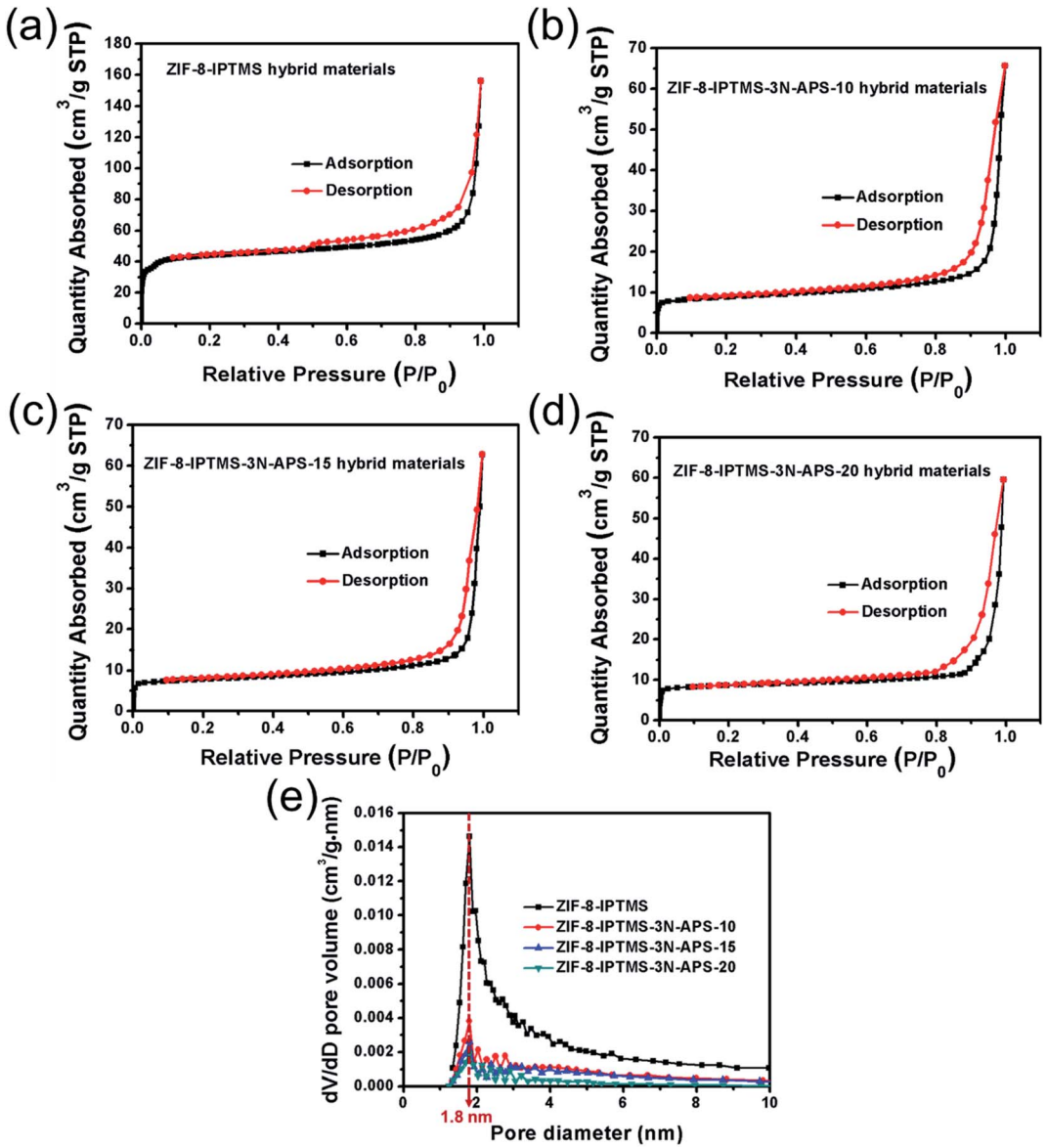

Fig. 4 N_2 adsorption/desorption isotherms of (a) ZIF-8-IPTMS, (b) ZIF-8-IPTMS-3N-APS-10, (c) ZIF-8-IPTMS-3N-APS-15, (d) ZIF-8-IPTMS-3N-APS-20, and (e) the BJH pore size distribution profiles of ZIF-8-IPTMS and ZIF-8-IPTMS-3N-APS.

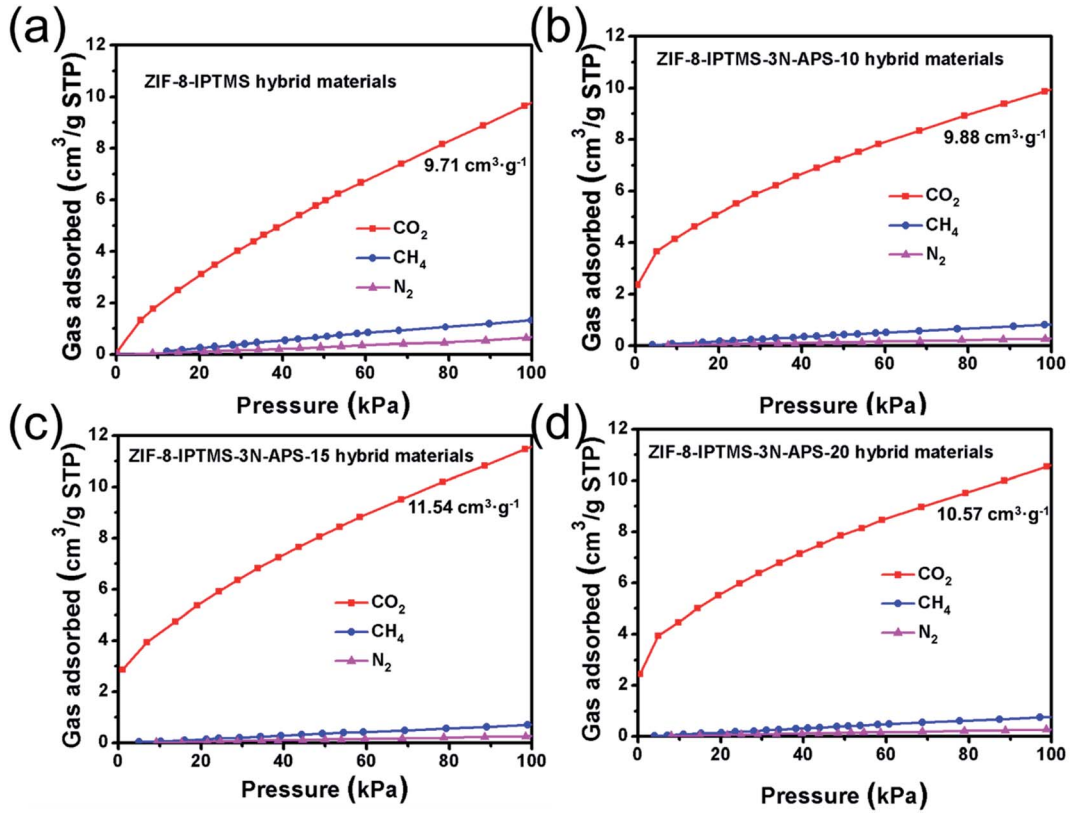

Fig. 5 CO_2, CH_4, and N_2 sorption isotherms for (a) ZIF-8-IPTMS, (b) ZIF-8-IPTMS-3N-APS-10, (c) ZIF-8-IPTMS-3N-APS-15, and (d) ZIF-8-IPTMS-3N-APS-20 conducted at 308 K.

ZIF-8-IPTMS, ZIF-8-IPTMS-3N-APS-10, ZIF-8-IPTMS-3N-APS-15, and ZIF-8-IPTMS-3N-APS-20 at 100 kPa were 9.71, 9.88, 11.54, and 10.57 $cm^3\ g^{-1}$, respectively. These slightly improved CO_2 adsorption capacities can be attributed to the abundant amino groups incorporated *via* the grafting of amine compounds.[46] In contrast, the insignificant CH_4 (*ca.* 0.67 $cm^3\ g^{-1}$) and N_2 (*ca.* 0.27 $cm^3\ g^{-1}$) of ZIF-8-IPTMS-3N-APS were adsorbed by the materials at 100 kPa. We could find that the CH_4 and N_2 adsorption capacities were markedly lower than that of the pristine ZIF-8-IPTMS, which were approximately 1.32 and 0.66 $cm^3\ g^{-1}$, respectively. This result could be mainly attributed to the significantly reduced surface area of the ZIF-8-IPTMS-3N-APS compared with the pristine ZIF-8-IPTMS. This distinction between the CO_2 adsorption capacity and the other two gas adsorption capacities indicates that the as-prepared ZIF-8-IPTMS-3N-APS, especially the ZIF-8-IPTMS-3N-APS-15, are potential materials for the separation of CO_2/N_2 and CO_2/CH_4 mixtures at 308 K.[47] More importantly, when employing the ZIF-8-IPTMS-3N-APS-15 in the fabrication of the ZIF-8 membrane, this difference in the adsorption capacities exerts an observable effect on the gas permeability of the resultant ZIF-8 membrane. Thus, the excellent CO_2 adsorption capacity exhibited by the ZIF-8-IPTMS-3N-APS-15 is beneficial to improving the CO_2 permeability, while negligible CH_4 and N_2 uptake can limit their permeabilities.

3.2. Breakthrough experiments conducted for the ZIF-8-IPTMS-3N-APS

To verify the efficient separation performance exhibited by the ZIF-8-IPTMS-3N-APS for the CO_2/CH_4 and CO_2/N_2 mixtures, real-time dynamic breakthrough experiments were conducted at 308 K. In these experiments, the feed gases consisted of CO_2/CH_4 (85/15 v/v) and CO_2/N_2 (85/15 v/v) mixtures. As shown in Fig. 6a–f, some roll-ups could be observed in these breakthrough curves, which can be attributed to the partial replacement of CH_4 or N_2 with CO_2 during the adsorption as competitive adsorptions between CO_2 and other components were expected.[47] It can also be observed from Fig. 6a–f that the acidic CO_2 was preferentially adsorbed on the ZIF-8-IPTMS-3N-APS when compared to the nonacidic N_2 or CH_4. Consequently, the ZIF-8-IPTMS-3N-APS was able to separate the CO_2/CH_4 (85/15 v/v) and CO_2/N_2 (85/15 v/v) mixtures efficiently owing to its preferential CO_2 adsorption. Even though these materials possess a considerable CO_2/CH_4 and CO_2/N_2 mixture separation performance, the energy consumption is inevitable for the regeneration of adsorbents, for example, ZIF-8-IPTMS-3N-APS, during the entire adsorption separation process. Fortunately, the ZIF-8-IPTMS-3N-APS can be theoretically used for the fabrication of the ZIF-8 membrane, whereby it can provide improvements to the membrane separation technique that can avoid the need for the regeneration process. Amino groups provide heterogeneous nucleation sites to grow dense ZIF-8

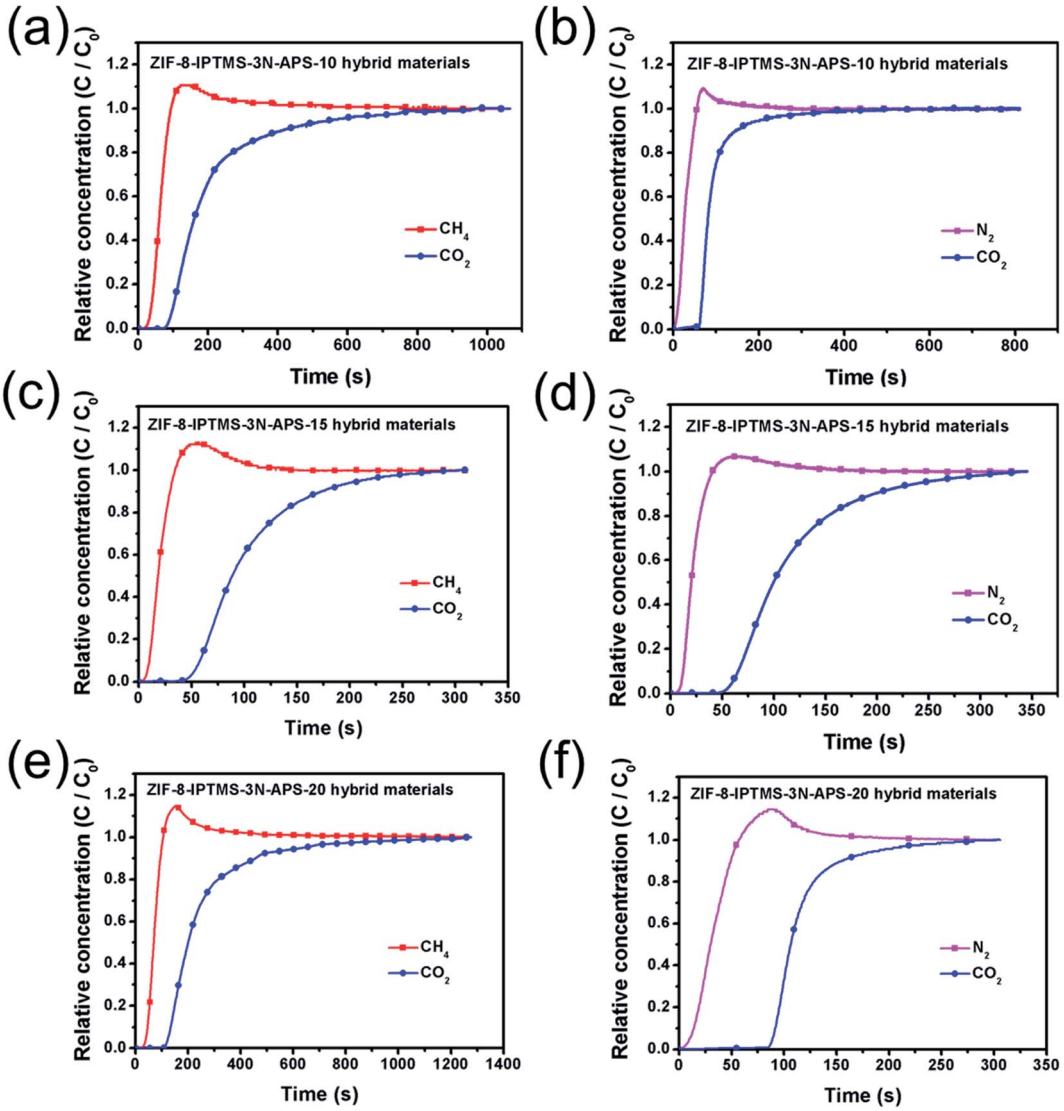

Fig. 6 Breakthrough profiles of (a) CO_2/CH_4 (15/85, v/v), (b) CO_2/N_2 (15/85, v/v) for ZIF-8-IPTMS-3N-APS-10, (c) CO_2/CH_4 (15/85, v/v), (d) CO_2/N_2 (15/85, v/v) for ZIF-8-IPTMS-3N-APS-15, and (e) CO_2/CH_4 (15/85, v/v), and (f) CO_2/N_2 (15/85, v/v) for ZIF-8-IPTMS-3N-APS-20 at 308 K.

membranes, and ZIF-8 membranes with a high CO_2 permeance can be obtained through the high CO_2 adsorption capacity of the ZIF-8-IPTMS-3N-APS.[14,16–18,48] Thus, abundant amino groups and a high CO_2 adsorption capacity are essential for the formation of a ZIF-8 membrane with a good CO_2 separation performance. Consequently, based on the collective results, the ZIF-8-IPTMS-3N-APS-15 was selected for the fabrication of a ZIF-8 membrane owing to the highest amine loading content and the highest CO_2 adsorption capacity among the rest of the as-synthesized ZIF-8-IPTMS-3N-APS.

3.3. Characterization of the as-fabricated ZIF-8 membrane

According to the SEM images (Fig. 7a and b), an extended and dense ZIF-8 membrane with a thickness of *ca.* 0.6 μm was successfully fabricated on the macroporous substrate with the aid of ZIF-8-IPTMS-3N-APS-15. Based on this result, depositing the ZIF-8-IPTMS-3N-APS-15 onto the surface of the macroporous substrate can facilitate the fabrication of an ultrathin ZIF-8 membrane, whereby such a membrane is expected to achieve a high gas permeance. The composition of the sample was analyzed using XRD, and the result is shown in Fig. 7c. It can be observed that the positions of the measured diffraction peaks were consistent with those in the simulated XRD spectrum of the ZIF-8 crystals. As such, this result shows that the sample comprises the pristine ZIF-8.

3.4. Single gas permeation and prolonged stability evaluation for the ZIF-8 membrane

Fig. 8a shows the ideal selectivity and single gas permeance of the as-synthesized ZIF-8 membrane. According to the result, the ideal CO_2 selectivities over N_2 and CH_4 were 4.67 and 6.02, respectively, which were higher than the corresponding Knudsen coefficients, that is, 1.24 and 1.66, respectively. Meanwhile, the CO_2 permeance at 35 °C and 0.1 MPa was retained at 4.75×10^{-6} mol m^{-2} s^{-1} Pa^{-1}. In addition, the ideal H_2/CH_4 selectivity reached 31.2, which was remarkably greater as compared to the

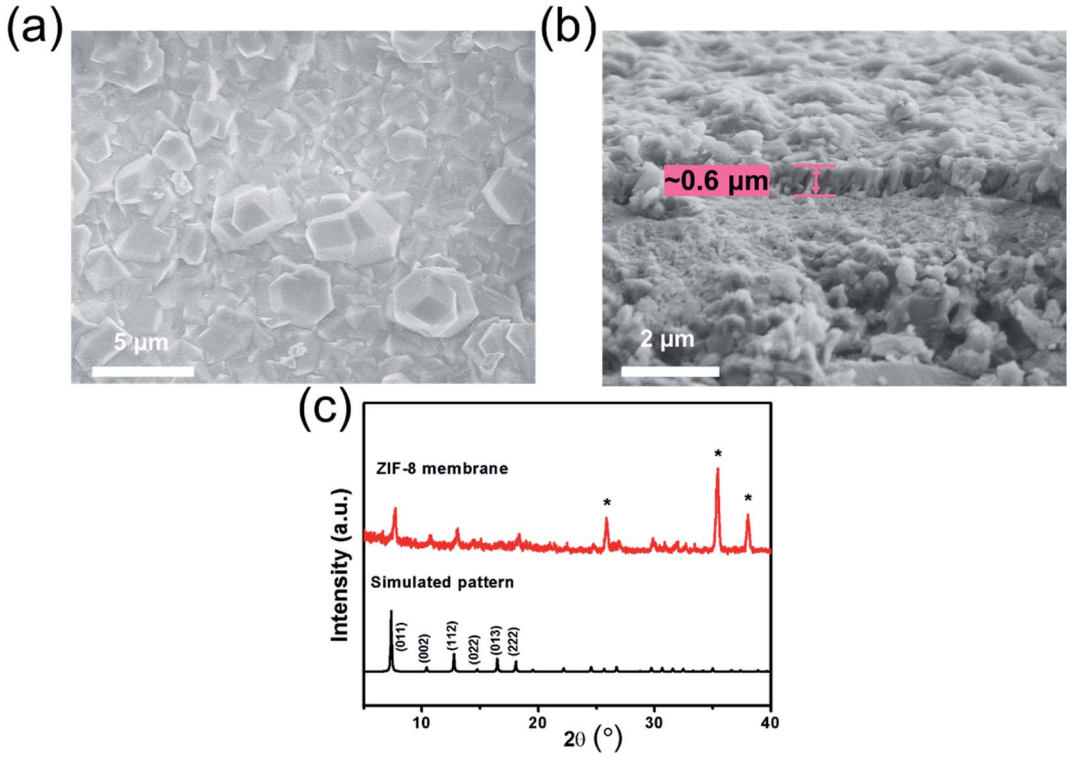

Fig. 7 SEM results of the (a) top perspective, (b) cross-sectional perspective, and (c) XRD patterns of the as-fabricated ZIF-8 membrane on the α-Al_2O_3 substrate modified with 1 wt% ZIF-8-IPTMS-3N-APS-15. The peaks of the α-Al_2O_3 support are indicated by *.

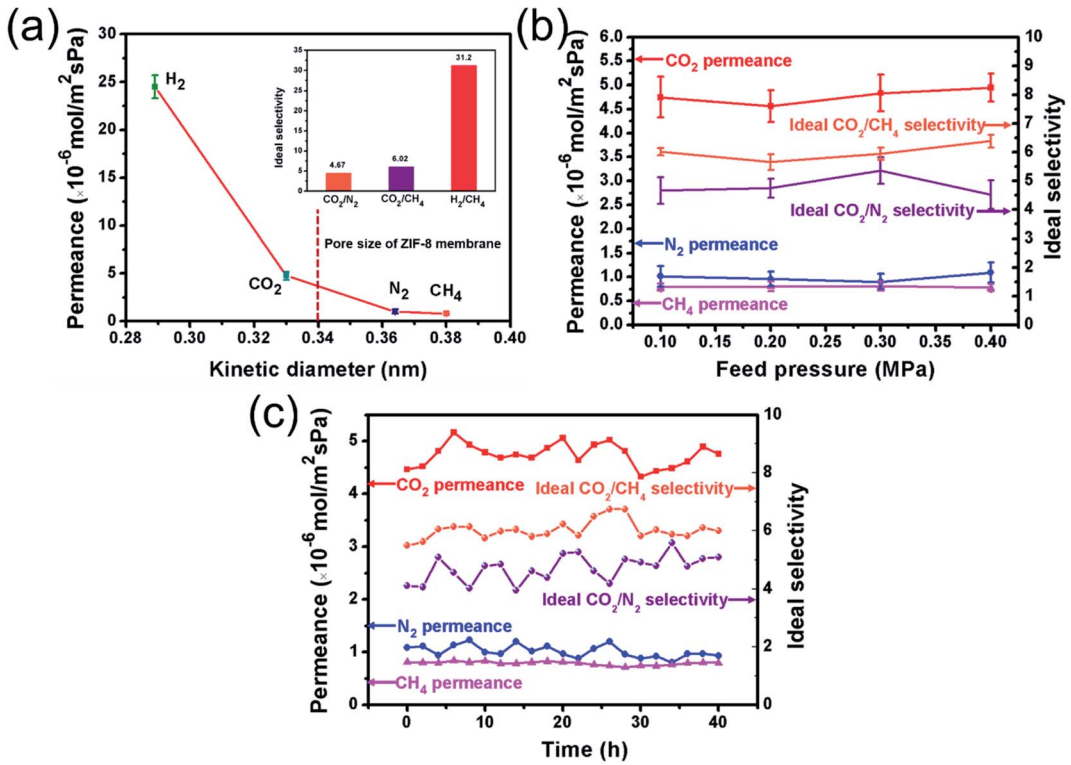

Fig. 8 (a) Single gas permeance, for example, CH_4, N_2, CO_2, and H_2, of the sample at 35 °C and 0.1 MPa. The inset shows the ideal selectivity. (b) Single gas permeances and ideal selectivity with the change in feed pressure (0.1–0.4 MPa, 35 °C). (c) Prolonged stability of the sample at 35 °C and 0.1 MPa.

Table 1 CO_2/N_2 and CO_2/CH_4 separation performances of the sample (prepared with 1 wt% ZIF-8-IPTMS-3N-APS-15) recorded at 35 °C and 0.1 MPa based on the W–K model[34,50–55]

				Single gas		Mixed gases (15 : 85 molar ratio)		
Membranes	Thickness (μm)	Temperature (°C)	Gas separation	CO_2 permeances (10^{-6} mol m^{-2} s^{-1} Pa^{-1})	Ideal selectivities	CO_2 permeances (10^{-6} mol m^{-2} s^{-1} Pa^{-1})	Separation factors	Ref.
1 wt% ZIF-8-IPTMS-3N-APS-15 deposition		35	CO_2/N_2	128 ± 13	2.54			This work
			CO_2/CH_4	128 ± 13	2.25			This work
ZIF-8	0.6	35	CO_2/N_2	4.75 ± 0.42	4.67	3.49 ± 0.26	3.74	This work
			CO_2/CH_4	4.75 ± 0.42	6.02	3.36 ± 0.17	4.91	This work
ZIF-8	0.9	35	CO_2/N_2	1.99	1.32			34
			CO_2/CH_4	1.99	1.69			
ZIF-8	20	150	CO_2/N_2	0.021	1.71			50
			CO_2/CH_4	0.021	3.38			
ZIF-8	20	250	CO_2/N_2	0.006	4.59			51
			CO_2/CH_4	0.006	8.85			
ZIF-8	6	30	CO_2/N_2	0.036	2.13			52
			CO_2/CH_4	0.036	2.42			
ZIF-8	30	25	CO_2/CH_4	0.027	3.6			53
ZIF-8	50	30	CO_2/CH_4			0.066	5.07	54
		50	CO_2/CH_4			0.053	4.22	
		70	CO_2/CH_4			0.047	4.51	
ZIF-8	5	23	CO_2/N_2	0.18	7.0			55
		80	CO_2/N_2	0.18	4.2			

corresponding Knudsen coefficient of 2.8. In this work, a significantly high H_2 permeance of 2.45×10^{-5} mol m^{-2} s^{-1} Pa^{-1} at 35 °C and 0.1 MPa was also recorded. This excellent separation performance of H_2/CH_4 is mainly due to two factors: (i) the ultrathin thickness of the ZIF-8 membrane; and (ii) the negligible CH_4 adsorption capacity of ZIF-8-IPTMS-3N-APS-15. Additionally, the single gas permeances and the ideal selectivity as a function of the feed pressure, which were from 0.1 to 0.4 MPa at 35 °C, are exhibited in Fig. 8b. We observed that there was negligible fluctuation in the gas permeance values of CH_4, N_2, and CO_2 with the change in feed pressure. This result indicates that the single gas separation performance of the as-synthesized ZIF-8 membrane is essentially independent of the feed pressure values. Furthermore, to investigate the continuous operation performance of the sample, a prolonged test was performed, and the result is shown in Fig. 8c. During the prolonged operation, both the gas permeance and ideal selectivity were relatively stable with slight changes. This result shows that the as-fabricated ZIF-8 membrane possesses an excellent durability, which suggests that it could be continuously operated without additional energy consumption. Thus, this result further demonstrates the feasibility and importance of incorporating an amine-based solid adsorbent into the fabrication of ZIF-8 membranes (supported on a macroporous substrate) in CO_2 separation.

3.5. Binary gas permeation test of the as-fabricated ZIF-8 membrane

Table 1 shows the results from the binary CO_2/N_2 (15/85, v/v) and CO_2/CH_4 (15/85, v/v) separation experiments for the sample. It is shown that the CO_2 permeance for the membrane was retained at 12.8×10^{-5} mol m^{-2} s^{-1} Pa^{-1} after depositing 1 wt% ZIF-8-IPTMS-3N-APS-15 onto the surface of the

Table 2 H_2/CH_4 separation performances of the sample (prepared with 1 wt% ZIF-8-IPTMS-3N-APS-15) at 35 °C and 0.1 MPa based on the W–K model

		H_2/CH_4 separation performances			
		Single gas		Mixed gases (50 : 50 molar ratio)	
Membrane	Thickness (μm)	H_2 permeances (10^{-6} mol m^{-2} s^{-1} Pa^{-1})	Ideal selectivity	H_2 permeances (10^{-6} mol m^{-2} s^{-1} Pa^{-1})	Separation factor
ZIF-8	0.6	24.5 ± 1.20	31.2	20.2 ± 0.49	24.7

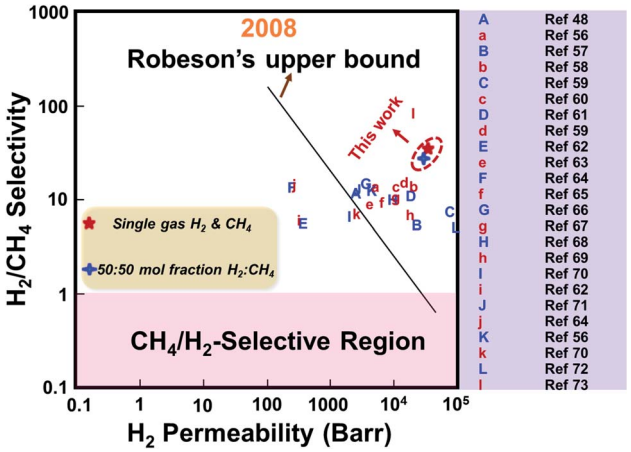

Fig. 9 Comparison of the single and binary H_2/CH_4 separation performances of the sample prepared in this work with the previously reported ZIF membranes and the upper limit. Lower-case and upper-case letters indicate single gas and binary gas permeation performance, respectively.[48,56–73]

macroporous substrate. Furthermore, the modified substrate exhibited inherent selectivities towards CO_2/N_2 (2.54) and CO_2/CH_4 (2.25), which may be due to the distinct differences in the CO_2 adsorption capacity as compared to N_2 and CH_4 exhibited by the microporous ZIF-8-IPTMS-3N-APS-15. The binary CO_2/N_2 (15/85, v/v) and CO_2/CH_4 (15/85, v/v) separation factors of the sample were 3.74 and 4.91, respectively, and the CO_2 permeances were 3.49 and 3.36 $\times$ 10^{-6} mol m^{-2} s^{-1} Pa^{-1}, respectively. Both the separation factor and CO_2 permeance obtained from the binary gas permeation experiment were lower than those obtained from the single gas permeation experiment. This occurrence is attributed to the competitive adsorption between the two types of gases during the binary gas permeation.[49] To further evaluate the performance, single and binary CO_2/N_2 and CO_2/CH_4 separation performances of the sample were compared with those of previously published ZIF-8 membranes. It is worth noting that the ideal CO_2/N_2 and CO_2/CH_4 selectivities of the ZIF-8 membrane reported in our previous work (prepared by depositing pristine ZIF-8-IPTMS onto the macroporous substrate) were 1.32 and 1.69, respectively, while the CO_2 permeance was 1.99 $\times$ 10^{-6} mol m^{-2} s^{-1} Pa^{-1} at 35 °C and 0.1 MPa.[34] When compared to the previously reported membrane, the CO_2 permeance and separation performance of the ZIF-8 membrane (prepared with ZIF-8-IPTMS-3N-APS-15) showed a significant enhancement. Furthermore, the performance of the ZIF-8 membrane prepared in this work was superior when compared to that of the other previously published ZIF-8 membranes.

Additionally, an equimolar binary H_2/CH_4 separation experiment was performed, and the result is exhibited in Table 2. According to the result, a H_2/CH_4 separation factor of 24.7 with a high H_2 permeance of 2.02 $\times$ 10^{-5} mol m^{-2} s^{-1} Pa^{-1} was achieved. The H_2 permeance was lower than that recorded from the single gas permeation experiment, and this could be attributed to the competitive gas adsorption behavior.[49] Furthermore, the single and binary H_2/CH_4 separation performances of the as-prepared ZIF-8 membrane and the previously reported ZIF membranes were compared and are summarized

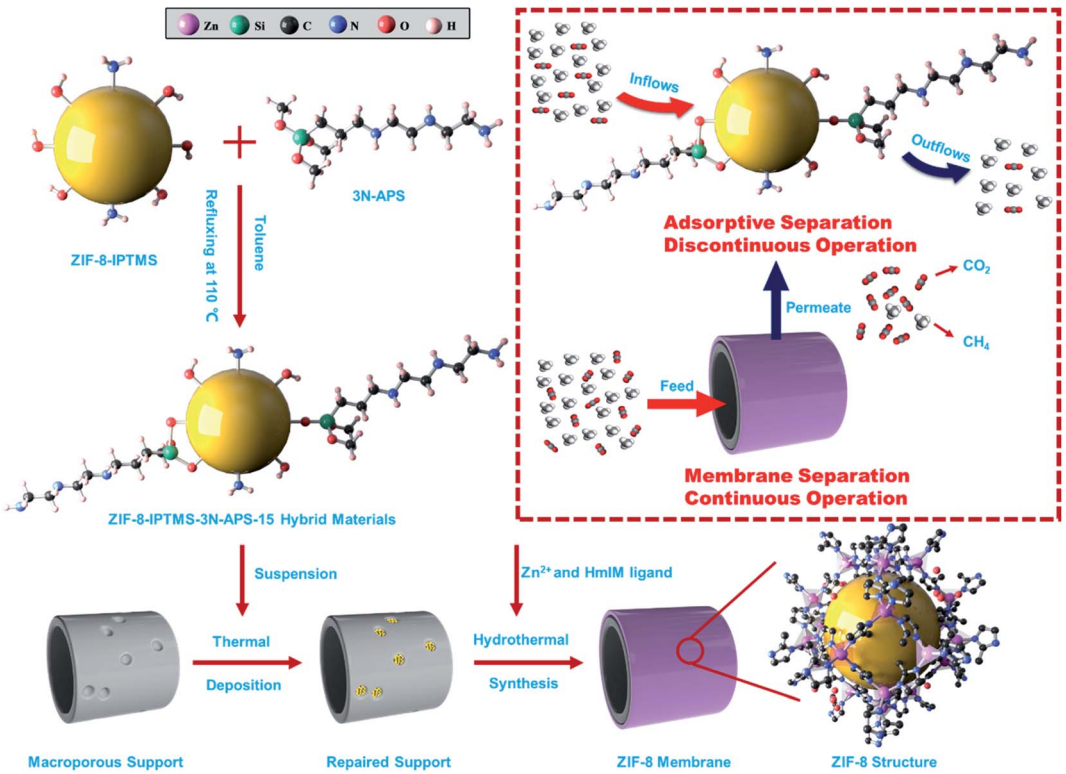

Fig. 10 Schematic diagram of the hybridization of the amine-based solid adsorbent and the ZIF-8 membrane.

in Fig. 9. Based on these findings, both the H_2 permeance and H_2/CH_4 separation performance of the as-prepared ZIF-8 membrane were superior compared to the majority of the previously reported ZIF membranes, and it exceeded the upper limit reported in 2008.

3.6. Elucidating the hybridization of the amine-based solid adsorbent and the ZIF-8 membrane

Fig. 10 illustrates the hybridization of amine-based solid adsorbents, that is, ZIF-8-IPTMS-3N-APS-15, with a ZIF-8 membrane. Briefly, the intrinsic hydroxyl groups present in pristine ZIF-8-IPTMS provide ample reaction sites for 3N-APS amine compounds to graft onto, and this can significantly increase the amino group content. As class 2 amine-based solid adsorbents, for example, ZIF-8-IPTMS-3N-APS-15, possess a considerable adsorptive CO_2 separation performance owing to their abundant and weakly alkaline amino groups, they can exert a strong attraction towards acidic CO_2. In this work, ZIF-8-IPTMS-3N-APS-15 was selected and incorporated during the preparation of the ZIF-8 membrane owing to the following reason: among the various ZIF-8-IPTMS-3N-APS, ZIF-8-IPTMS-3N-APS-15 possessed the highest amino group content and highest CO_2 adsorption capacity, which can provide ample heterogeneous nucleation sites for ZIF-8 membranes to grow. Thus, based on the collective results, the as-prepared ZIF-8 membrane was able to operate continuously, and it could also exhibit an enhanced CO_2 separation performance owing to the considerable CO_2 adsorption capacity exhibited by ZIF-8-IPTMS-3N-APS-15.

4. Conclusion

The porous ZIF-8-IPTMS-3N-APS was successfully synthesized in this work, and it was then used in CO_2 adsorption separation and the subsequent preparation of the ZIF-8 membrane for CO_2 separation. Considerable CO_2 adsorption separation performances were achieved using the as-prepared ZIF-8-IPTMS-3N-APS owing to their high CO_2 and negligible N_2 and CH_4 adsorption capacities. However, to achieve the continual operation of CO_2 adsorption separation, these adsorbents have to regenerate which involves energy consumption. To avoid the need for regeneration, the ZIF-8-IPTMS-3N-APS-15 was selected and incorporated in the fabrication of the ZIF-8 membrane. This is because the ZIF-8-IPTMS-3N-APS-15 possesses the highest amine-loading content and the highest CO_2 adsorption capacity among the rest of the as-prepared ZIF-8-IPTMS-3N-APS. As shown by the prolonged stability test, the as-fabricated ZIF-8 membrane was able to operate continuously without the need for regeneration. Furthermore, excellent CO_2/N_2, CO_2/CH_4, and H_2/CH_4 separation performances were achieved, which could mainly be ascribed to the 0.6 μm ultrathin ZIF-8 membrane, and the high CO_2 and negligible N_2 and CH_4 adsorption capacities of the ZIF-8-IPTMS-3N-APS-15. As such, the as-proposed strategy for incorporating an amine-based solid adsorbent into the preparation process of ZIF-8 membranes may present a promising method for the future preparation of tubular MOF membranes.

Conflicts of interest

The authors declare no conflicts of interest.

Acknowledgements

The authors gratefully acknowledge financial support received from the National Natural Science Foundation of China (21576011).

References

1 I. S. Omodolor, H. O. Otor, J. A. Andonegui, B. J. Allen and A. C. Alba-Rubio, *Ind. Eng. Chem. Res.*, 2020, **59**, 17612–17631.
2 W. Zhang, H. Liu, Y. Sun, J. Cakstins, C. Sun and C. E. Snape, *Appl. Energy*, 2016, **168**, 394–405.
3 S. Zhou, M. Wang, S. Wei, S. Cao, Z. Wang, S. Liu, D. Sun and X. Lu, *Mater. Today Phys.*, 2021, **16**, 100301.
4 G. Ji, and M. Zhao, in *Recent Advances in Carbon Capture and Storage*, InTechOpen, 2017, pp. 59–90.
5 I. Kammakakam, Y. N. Sang and T. H. Kim, *RSC Adv.*, 2016, **6**, 31083–31091.
6 M. J. C. Ordoñez, K. J. Balkus, J. P. Ferraris and I. H. Musselman, *J. Membr. Sci.*, 2010, **361**, 28–37.
7 S. Kasahara, E. Kamio, T. Ishigami and H. Matsuyama, *Chem. Commun.*, 2012, **48**, 6903–6905.
8 B. Liu, R. Zhou, N. Bu, Q. Wang, S. Zhong, B. Wang and K. Hidetoshi, *J. Membr. Sci.*, 2017, **524**, 12–19.
9 D. Q. Vu, W. J. Koros and S. J. Miller, *Ind. Eng. Chem. Res.*, 2002, **41**, 367–380.
10 P. Natarajan, B. Sasikumar, S. Elakkiya, G. Arthanareeswaran, A. F. Ismail, W. Youravong and E. Yuliwati, *J. Nat. Gas Sci. Eng.*, 2021, **86**, 103720.
11 T. T. Moore, R. Mahajan, D. Q. Vu and W. J. Koros, *AIChE J.*, 2004, **50**, 311–321.
12 H. T. Kwon and H. K. Jeong, *J. Am. Chem. Soc.*, 2013, **135**, 10763–10768.
13 R. Banerjee, A. Phan, B. Wang, C. Knobler, H. Furukawa, M. O'Keeffe and O. M. Yaghi, *Science*, 2008, **319**, 939–943.
14 Y. Gao, Z. Qiao, S. Zhao, Z. Wang and J. Wang, *J. Mater. Chem. A*, 2018, **6**, 3151–3161.
15 J. S. Tuninetti, M. Rafti and O. Azzaroni, *RSC Adv.*, 2015, **5**, 73958–73962.
16 X. Yang, H. Du, Y. Lin, L. Song, Y. Zhang, X. Gao, C. Kong and L. Chen, *J. Membr. Sci.*, 2016, **506**, 31–37.
17 N. A. H. M. Nordin, S. M. Racha, T. Matsuura, N. Misdan, N. A. A. Sani, A. F. Ismail and A. Mustafa, *RSC Adv.*, 2015, **5**, 43110–43120.
18 R. Abedini, M. Omidkhah and F. Dorosti, *RSC Adv.*, 2014, **4**, 36522–36537.
19 B. Sasikumar, S. Bisht, G. Arthanareeswaran, A. F. Ismail and M. H. D. Othman, *Sep. Purif. Technol.*, 2021, **264**, 118471.
20 S. Choi, J. H. Drese, P. M. Eisenberger and C. W. Jones, *Environ. Sci. Technol.*, 2011, **45**, 2420–2427.
21 D. Lv, R. Shi, Y. Chen, Y. Chen, H. Wu, X. Zhou, H. Xi, Z. Li and Q. Xia, *Ind. Eng. Chem. Res.*, 2018, **57**, 12215–12224.

22 P. Bollini, S. A. Didas and C. W. Jones, *J. Mater. Chem.*, 2011, **21**, 15100–15120.
23 A. Goeppert, M. Czaun, G. K. S. Prakash and G. A. Olah, *Cheminform*, 2012, **5**, 7833–7853.
24 J. C. Hicks, J. H. Drese, D. J. Fauth, M. L. Gray, G. Qi and C. W. Jones, *J. Am. Chem. Soc.*, 2008, **130**, 2902–2903.
25 F. Y. Chang, K. J. Chao, H. H. Cheng and C. S. Tan, *Sep. Purif. Technol.*, 2009, **70**, 87–95.
26 H. Y. Huang, R. T. Yang, D. Chinn and C. L. Munson, *Ind. Eng. Chem. Res.*, 2003, **42**, 2427–2433.
27 H. Yang, Z. Xu, M. Fan, R. Gupta, R. B. Slimane, A. E. Bland and I. Wright, *J. Environ. Sci.*, 2008, **20**, 14–27.
28 J. Zhang, P. A. Webley and P. Xiao, *Energy Convers. Manage.*, 2008, **49**, 346–356.
29 C. Zhao, X. Chen, E. J. Anthony, X. Jiang, L. Duan, Y. Wu, W. Dong and C. Zhao, *Prog. Energy Combust. Sci.*, 2013, **39**, 515–534.
30 V. I. Agueda, J. A. Delgado, M. A. Uguina, P. Brea, A. I. Spjelkavik, R. Blom and C. Grande, *Chem. Eng. Sci.*, 2015, **124**, 159–169.
31 V. M. A. Melgar, J. Kim and M. R. Othman, *J. Ind. Eng. Chem.*, 2015, **28**, 1–15.
32 Y. Zhao, Y. Wei, L. Lyu, Q. Hou, J. Caro and H. Wang, *J. Am. Chem. Soc.*, 2020, **142**, 20915–20919.
33 Y. Yue, Z. A. Qiao, X. Li, A. J. Binder, E. Formo, Z. Pan, C. Tian, Z. Bi and S. Dai, *Cryst. Growth Des.*, 2013, **13**, 1002–1005.
34 Y. Qin, L. Xu, L. Liu and Z. Ding, *Ind. Eng. Chem. Res.*, 2021, **60**, 1387–1395.
35 N. Hiyoshi, K. Yogo and T. Yashima, *Microporous Mesoporous Mater.*, 2005, **84**, 357–365.
36 D. Liu, X. Ma, H. Xi and Y. S. Lin, *J. Membr. Sci.*, 2014, **451**, 85–93.
37 Z. Tao, S. Yang, D. K. Choi and K. H. Row, *Korean J. Chem. Eng.*, 2010, **27**, 1910–1915.
38 J. Zhao, M. Milanova, M. M. C. G. Warmoeskerken and V. Dutschk, *Colloids Surf., A*, 2012, **413**, 273–279.
39 P. J. E. Harlick and A. Sayari, *Ind. Eng. Chem. Res.*, 2007, **46**, 446–458.
40 C. Lu, H. Bai, B. Wu, F. Su and J. F. Hwang, *Energy Fuels*, 2008, **22**, 3050–3056.
41 B. T. Low, T. S. Chung, H. Chen, Y. C. Jean and K. P. Pramoda, *Macromolecules*, 2009, **42**, 7042–7054.
42 Y. G. Ko, H. J. Lee, J. Y. Kim and U. S. Choi, *ACS Appl. Mater. Interfaces*, 2014, **6**, 12988–12996.
43 H. Y. Huang, R. T. Yang, D. Chinn and C. L. Munson, *Ind. Eng. Chem. Res.*, 2003, **42**, 2427–2433.
44 Y. Zhou and C. J. Liu, *Plasma Chem. Plasma Process.*, 2011, **31**, 499–506.
45 A. Schejn, L. Balan, V. Falk, L. Aranda, G. Medjahdi and R. Schneider, *Crystengcomm*, 2014, **16**, 4493–4500.
46 J. Q. Zhao, F. Simeon, Y. J. Wang, G. S. Luo and T. A. Hatton, *RSC Adv.*, 2012, **2**, 6509–6519.
47 D. Lv, J. Chen, K. Yang, H. Wu, Y. Chen, C. Duan, Y. Wu, J. Xiao, H. Xi, Z. Li and Q. Xia, *Chem. Eng. J.*, 2019, **375**, 122074.
48 K. Huang, Z. Dong, Q. Li and W. Jin, *Chem. Commun.*, 2013, **49**, 10326–10328.
49 J. Wu, J. Liu and T. S. Chung, *Adv. Sustainable Syst.*, 2018, **2**, 1800044.
50 Q. Liu, N. Wang, J. Caro and A. Huang, *J. Am. Chem. Soc.*, 2013, **135**, 17679–17682.
51 A. Huang, Q. Liu, N. Wang, Y. Zhu and J. Caro, *J. Am. Chem. Soc.*, 2014, **136**, 14686–14689.
52 X. Zhang, Y. Liu, S. Li, L. Kong, H. Liu, Y. Li, W. Han, K. L. Yeung, W. Zhu, W. Yang and J. Qiu, *Chem. Mater.*, 2014, **26**, 1975–1981.
53 Y. Pan, B. Wang and Z. Lai, *J. Membr. Sci.*, 2012, **421–422**, 292–298.
54 L. S. Lai, Y. F. Yeong, T. L. Chew, K. K. Lau and M. S. Azmi, *J. Nat. Gas Sci. Eng.*, 2016, **34**, 509–519.
55 Y. Miao, D. T. Lee, M. D. Mello, M. K. Abdel-Rahman, P. Corkery, J. A. Boscoboinik, D. H. Fairbrother and M. Tsapatsis, *Chem. Commun.*, 2021, **57**, 5250–5253.
56 M. Shah, M. C. McCarthy, S. Sachdeva, A. K. Lee and H.-K. Jeong, *Ind. Eng. Chem. Res.*, 2012, **51**, 2179–2199.
57 H. Deng, C. J. Doonan, H. Furukawa, R. B. Ferreira, J. Towne, C. B. Knobler, B. Wang and O. M. Yaghi, *Science*, 2010, **327**, 846–850.
58 H. Furukawa, K. E. Cordova, M. O'Keeffe and O. M. Yaghi, *Science*, 2013, **341**, 1230444.
59 Z. Kang, L. Fan, S. Wang, D. Sun, M. Xue and S. Qiu, *CrystEngComm*, 2017, **19**, 1601–1606.
60 Z. Wang and S. M. Cohen, *J. Am. Chem. Soc.*, 2007, **129**, 12368–12369.
61 J. H. Cavka, S. Jakobsen, U. Olsbye, N. Guillou, C. Lamberti, S. Bordiga and K. P. Lillerud, *J. Am. Chem. Soc.*, 2008, **130**, 13850–13851.
62 J. Gascon, F. Kapteijn, B. Zornoza, V. Sebastian, C. Casado and J. Coronas, *Chem. Mater.*, 2012, **24**, 2829–2844.
63 E. Shamsaei, X. Lin, Z.-X. Low, Z. Abbasi, Y. Hu, J. Z. Liu and H. Wang, *ACS Appl. Mater. Interfaces*, 2016, **8**, 6236–6244.
64 A. Phan, C. J. Doonan, F. J. Uribe-Romo, C. B. Knobler, M. O'keeffe and O. M. Yaghi, *Acc. Chem. Res.*, 2010, **43**, 58–67.
65 J. Li, W. Cao, Y. Mao, Y. Ying, L. Sun and X. Peng, *CrystEngComm*, 2014, **16**, 9788–9791.
66 Y. Liu, Z. Ng, E. A. Khan, H.-K. Jeong, C.-B. Ching and Z. Lai, *Microporous Mesoporous Mater.*, 2009, **118**, 296–301.
67 B. Chen, L. Wang, F. Zapata, G. Qian and E. B. Lobkovsky, *J. Am. Chem. Soc.*, 2008, **130**, 6718–6719.
68 H. T. Kwon and H.-K. Jeong, *J. Am. Chem. Soc.*, 2013, **135**, 10763–10768.
69 J. C. Tan, T. D. Bennett and A. K. Cheetham, *Proc. Natl. Acad. Sci.*, 2010, **107**, 9938–9943.
70 C. Yuan, Q. Liu, H. Chen and A. Huang, *RSC Adv.*, 2014, **4**, 41982–41988.
71 P. Nian, Y. Cao, Y. Li, X. Zhang, Y. Wang, H. Liu and X. Zhang, *CrystEngComm*, 2018, **20**, 2440–2448.
72 H. Bux, C. Chmelik, R. Krishna and J. Caro, *J. Membr. Sci.*, 2011, **369**, 284–289.
73 Y. Li, F. Liang, H. Bux, W. Yang and J. Caro, *J. Membr. Sci.*, 2010, **354**, 48–54.